Meteorological influence on surface ozone trends in China: Assessing

uncertainties caused by multi-dataset and multi-method

- 3 Xueqing Wang¹, Jia Zhu^{1*}, Guanjie Jiao¹, Xi Chen¹, Zhenjiang Yang¹, Lei Chen^{1,2}, Xipeng Jin¹, and Hong
- 4 Liao¹

10

- 5 ¹Jiangsu Key Laboratory of Atmospheric Environment Monitoring and Pollution Control, Jiangsu Collaborative Innovation
- 6 Centre of Atmospheric Environment and Equipment Technology, Joint International Research Laboratory of Climate and
- 7 Environment Change, School of Environmental Science and Engineering, Nanjing University of Information Science and
- 8 Technology, Nanjing, 210044, China
- 9 2State Environmental Protection Key Laboratory of Sources and Control of Air Pollution Complex, Beijing, China
- 11 Correspondence: Jia Zhu (jiazhu@nuist.edu.cn)
- 12 **Abstract.** China has witnessed notable increases in surface ozone (O₃) concentrations since 2013, with meteorology identified
- 13 as a critical driver. However, meteorological contributions vary with different meteorological datasets and analytical methods,
- 14 and their uncertainties remain unassessed. This study leveraged decadal observational maximum daily 8-hour average O₃
- 15 records (2013–2022) across China, revealing intensified nationwide O₃ pollution with increasing O₃ trends of 0.79–1.31 ppb
- 16 yr⁻¹ during four seasons. We gave special focus on uncertainties of meteorology-driven O₃ trends by using diverse
- 17 meteorological datasets (ERA5, MERRA2, FNL) and diverse analytical methods (Multiple Linear Regression, Random Forest,
- 18 GEOS-Chem model). A useful statistic (coefficient of variation, CV) was adopted as an uncertainty quantification metric. For
- 19 multi-dataset analysis, models driven by different meteorological datasets exhibited the maximum meteorology-driven O₃
- 20 trend (+0.55 ppb yr⁻¹, multi-dataset mean) with the highest consistency (CV=0.25) in spring. The FNL-driven model always
- 21 obtained larger trends compared to ERA5 and MERRA2, which could be attributed to inability to accurately evaluate planetary
- 22 boundary layer height in FNL dataset. For multi-method analysis, three methods demonstrated optimal consistency in winter
- 23 (CV=0.40) and the worst consistency in summer (CV=2.00). The meteorology-driven O₃ trends obtained from GEOS-Chem
- 24 model were almost smaller than those obtained by other two methods, partly resulting from higher simulated O₃ values before
- 25 2018. Overall, all analyses driven by diverse meteorological datasets and analytical methods drew a robust conclusion that
- 26 meteorological conditions almost boosted O₃ increases during all seasons; the uncertainties caused by different analytical
- 27 methods were larger than those caused by diverse meteorological datasets.

28

29

Keywords: Meteorological impact, O₃ trend, Uncertainty

1 Introduction

30

31 Since 2013, the Chinese government has implemented a series of policies to mitigate air pollution resulting from the rapid 32 industrial and urban expansion, such as the "Air Pollution Prevention and Control Action Plan" (Wang, 2021). Several criteria 33 air pollutants exhibited decreases due to the emission control efforts, but not ozone (O₃) (Qi et al., 2023; Shen et al., 2020).In China, O₃ concentrations were increased by 50–124 µg m⁻³ from 2015 to 2022 (Yao et al., 2024). The formation of surface O₃ 34 35 depends nonlinearly on its precursors and is strongly influenced by meteorological conditions and anthropogenic emissions (Wang et al., 2017). The impact of emission-related factors on O₃ increases in China over the past decade has been extensively 36 debated, including the ineffective control of volatile organic compounds (VOCs) emissions, the heightened O₃ photochemical 37 38 production due to the rapid decrease in PM_{2.5}, and the reduced nitric oxide (NO) titration effect (Li et al., 2019, 2022; Lin et 39 al., 2021a; Liu and Wang, 2020b; Ren et al., 2022).

40 Meteorological conditions also play a crucial role in shaping surface O₃ trends (Liu et al., 2023; Lu et al., 2019b), resulting in 41 increased O₃ concentrations during warm seasons over most of the United States, the European Union, and China from 2014 42 to 2019 (Lyu et al., 2023). In China, the meteorological impacts on O₃ levels may be comparable to the anthropogenic 43 contributions (Li et al., 2020; Liu and Wang, 2020a). From 2013 to 2018, meteorology could account for 43% of the daily variability in summer surface O₃ concentrations in eastern China (Han et al., 2020). Adverse meteorological conditions were 44 45 identified as the cause of the worsening O₃ trends during 2015–2020 in Beijing-Tianjin-Hebei (BTH), Yangtze River Delta (YRD), and Pearl River Delta (PRD) regions (Hu et al., 2024b). In YRD, Dang et al. (2021) found that meteorological factors 46 contributed 84% of the O₃ increase during the summers of 2012–2017. In PRD, meteorological conditions contributed 83% of 47 48 the increasing O₃ trends during the summers of 2015–2019 (Mousavinezhad et al., 2021). After 2019, meteorological 49 conditions tended to improve O₃ air quality (Liu et al., 2023; Wang et al., 2023). Compared to 2019, the wetter and cooler 50 meteorological conditions in 2020 reduced O₃ concentrations by 2.9 ppb in eastern China (Yin et al., 2021). However, during 51 2022's summer, a notable rebound in O₃ levels occurred with O₃ concentrations rising by 12-15 ppb in China compared to 52 2021, which was attributable to the extreme heatwave events (Qiao et al., 2024). With climate change, the frequency of extreme 53 O₃ pollution events is expected to increase (Gao et al., 2023; Ji et al., 2024). Given the shifted meteorological effects on O₃ 54 and climate change, it is imperative to conduct O₃-Meteorology researches focusing on longer time frames to gain deeper 55 insights into the long-term changes in O₃ concentrations (Wang et al., 2024a).

Studies conducted over the past six years to determine the meteorological influence on the surface O₃ trend have been systematically reviewed, as documented in **Table S1**. The meteorological influence on surface O₃ concentrations is commonly assessed by using the traditional statistical model (TSM), machine learning model (MLM), and chemical transport model (CTM), driven by reanalysis meteorological products such as the fifth-generation European Centre for Medium-Range Weather Forecasts atmospheric reanalysis of the global climate (ERA5), the Modern-Era Retrospective Analysis for Research and Applications, version 2 (MERRA2), and the National Centres for Environmental Prediction (NCEP) Final Operational 62 Global Analysis data (FNL). Although several studies have demonstrated that meteorological impacts derived from CTM

63 results can corroborate the results of TSM (Liu et al., 2023; Yan et al., 2024) or MLM (Ni et al., 2024; Yin et al., 2021),

64 uncertainties in the determination of meteorological effects on surface O₃ concentrations cannot be neglected. For example,

65 Pan et al. (2023) reported that the meteorological impact on O₃ trends in Beijing during 2013–2020 was +0.52 ppb yr⁻¹, which

66 is only half of the value estimated by Gong et al. (2022).

71

82

85

89 90

93

67 Uncertainties in quantifying the drivers of O₃ trends can be ascribed to the discrepancies between different meteorological

datasets and between different methods (Guo et al., 2021; Weng et al., 2022; Yao et al., 2024). Regarding the uncertainty

69 caused by different meteorological datasets, the meteorologically driven annual variations of O₃ concentrations from 2017 to

70 2019 identified by the MERRA2-driven TSM are not consistent with the ERA5-driven TSM during the summer of YRD (Hu

et al., 2024a; Qian et al., 2022). During the summers of 2013–2019 in YRD, Li et al. (2019) reported a trend of +0.7 ppb yr⁻¹

72 in meteorology-driven O₃ concentrations using the MERRA2-driven TSM, while the trend of Yan et al. (2024) was -0.3 μg

73 m⁻³ yr⁻¹ using the ERA5-driven TSM. Regarding the uncertainty caused by different methods, the meteorology-driven O₃ trend

74 identified by MLM for 2019–2021 was 2.4 times larger than that identified by CTM based on the same meteorological dataset

75 input (MERRA2) in the North China Plain (NCP) during summer (Wang et al., 2024a). In BTH, from 2021 to 2022, Luo et al.

76 (2024) identified a negative meteorological contribution based on the ERA5-driven MLM, while Yan et al. (2024) suggested

77 a positive contribution (+4.3 μg m⁻³) based on the ERA5-driven TSM during summer.

78 On the basis of the above-mentioned, large uncertainties caused by multi-dataset or multi-method exist in O₃-Meteorology

79 analyses. However, available intercomparisons of O₃ analyses mainly focused on predicting the O₃ concentrations. For

80 example, Wang et al. (2024b) and Weng et al. (2023) compared the differences in O₃ concentration prediction caused by

81 different datasets and models, respectively. The uncertainties in quantifying the meteorological contributions to O₃ trends

caused by multi-dataset and multi-method remain unassessed. In addition, previous studies have predominantly focused on

83 summer O₃ pollution, although reports indicate an extension of the O₃ pollution season to winter and spring across major

84 clusters in China (Cao et al., 2024a; Li et al., 2021) and an unfavourable meteorological impact on O₃ air quality in spring and

winter in BTH (Luo et al., 2024). It is essential to conduct an intercomparison of meteorology-driven O₃ quantification using

86 multi-dataset and multi-method across all seasons.

87 This study utilised 10-year (2013–2022) surface O₃ observations in China to investigate long-term O₃ trends and quantify the

88 meteorological influence on O₃ trends using diverse meteorological datasets and analytical methods. Figure 1 shows the

framework, and the main objectives were: (1) to assess uncertainties in identifying the meteorological influences caused by

multi-dataset. This was achieved by employing the TSM (i.e. multiple linear regression, MLR) driven by different reanalysis

91 meteorological products (i.e. ERA5, MERRA2, and FNL); (2) to assess uncertainties in identifying meteorological effects

92 caused by multi-method. This was achieved by establishing three models corresponding to TSM (i.e. MLR), MLM (i.e. random

forest, RF), and CTM (i.e. GEOS-Chem, GC), each driven by the MERRA2 product; (3) to calculate the mean of meteorology-

94 driven O₃ trends driven by three datasets (multi-dataset mean) and three methods (multi-method mean), so as to to derive 95 relatively robust results.

Our paper is structured as follows: Section 2 briefly introduces the details of surface O₃ observations and different meteorological datasets, as well as the framework of three methods, namely MLR, RF, and GC. The quantification of the uncertainties in the meteorology-driven O₃ trends caused by multi-dataset and multi-method is presented in Section 3. Section 4 concludes the paper. The findings of this study provide a scientific foundation for developing regional and seasonal strategies to mitigate and manage O₃ pollution in China.

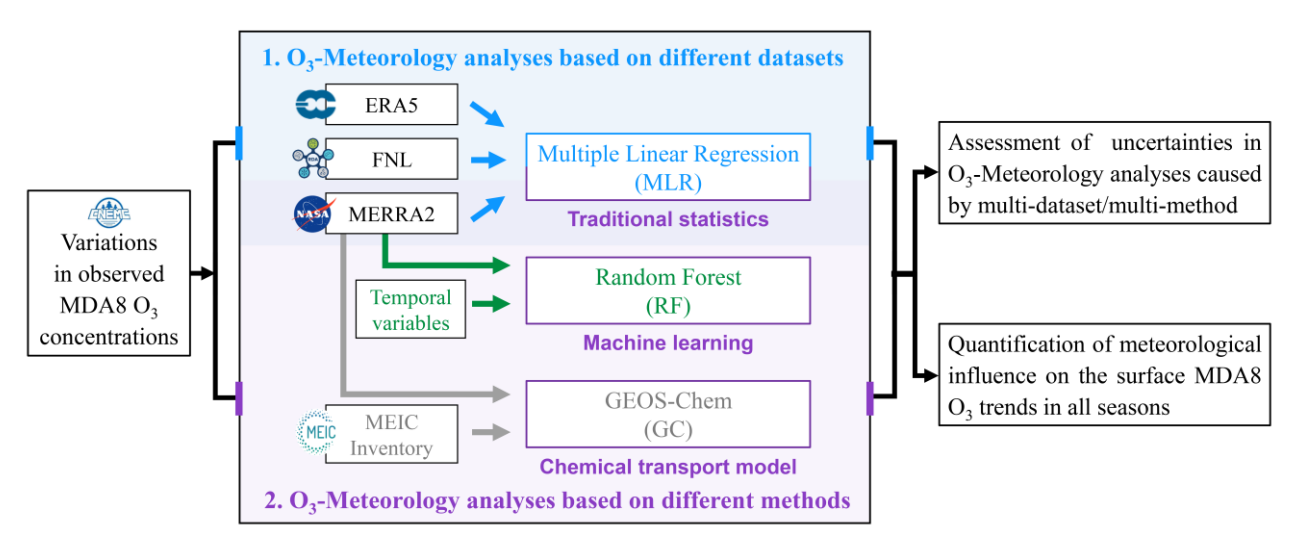


Figure 1. The framework of the uncertainty assessment in this study.

2 Data and Methods

2.1 Surface O₃ and meteorological data sources

Hourly surface O₃ observations from over 1000 state-controlled stations operated by the China National Environmental Monitoring Centre from 2013 to 2022 were used to analyse the long-term O₃ trends across all seasons: spring (March-April-May), summer (June-July-August), autumn (September-October-November), and winter (December-January-February). The maximum daily 8-hour average (MDA8) O₃ was calculated as an air quality indicator after filtering out abnormal data using the z-scores method. For detailed information on data quality control, refer to He et al. (2017).

In this study, we selected three widely used reanalysis products to assess the uncertainties caused by different meteorological datasets. Variables during 2013–2022 from ERA5, MERRA2, and FNL, as detailed in **Table S2**, were selected as meteorological inputs for building MLR models. These reanalyses have spatial resolutions of 0.25°×0.25°, 0.625°×0.5°, and

- 113 1°×1° on a global latitude-longitude grid, respectively. In Section 3.2, we have also incorporated the NCEP FNL reanalysis
- 114 product with a spatial resolution of 0.25°×0.25° (FNL025) for the period 2016–2022 to explore the effect of spatial resolution
- on the analysis of uncertainties caused by multi-dataset.

116 2.2 Methods for obtaining long-term series and meteorological influence

117 2.2.1 Kolmogorov–Zurbenko (KZ) filter

- 118 The KZ filter, known for its ability to extract low frequency signals from time series data and handle missing values, has been
- extensively applied in-to analysing air quality variations (Eskridge et al., 1997; Rao and Zurbenko, 1994; Wise and Comrie,
- 120 2005). This filter is particularly useful in studying variations in air quality over time. The original time series of air pollutants
- 121 or meteorological variables (X(t)) can be decomposed by the KZ filter into the following form:

$$X(t) = X_{ST}(t) + X_{SN}(t) + X_{LT}(t)$$
(1)

$$X_{LT}(t) = KZ_{(365.3)}X(t) \tag{2}$$

$$X_{BL}(t) = KZ_{(15.5)}X(t) \tag{3}$$

$$X_{ST}(t) = X(t) - X_{BL}(t) \tag{4}$$

- 122 In the decomposition process, X(t) represents the original daily time series, while $X_{ST}(t)$, $X_{SN}(t)$, and $X_{LT}(t)$ denote the
- short-term, seasonal, and long-term components, respectively. The baseline component, $X_{BL}(t)$, is defined as the sum of
- 124 $X_{SN}(t)$ and $X_{LT}(t)$. The $KZ_{(p,q)}$ filter executes q iterations with p as the moving average window length of X(t) series.
- Specially, $X_{LT}(t)$ is derived using the $KZ_{(365,3)}$ filter, capturing long-term changes with periods exceeding 1.7 years. $X_{BL}(t)$
- 126 is obtained through the $KZ_{(15,5)}$ filter, encompassing both seasonal and long-term components. $X_{ST}(t)$ represents short-term
- 127 fluctuations with period less than 33 days in the original time series. $X_{SN}(t)$ is derived as the difference between $X_{BL}(t)$ and
- $X_{LT}(t)$, corresponding to seasonal variation on a timescale of months. The KZ filter can fill in missing values by using iterated
- moving average technique. Although not all of the ozone measurement sites were active over the entire period 2013–2022,
- missing value problems can be handled for most stations after we conduct three iterations with 365-day moving average.
- 131 In this study, all statistical analyses were performed at the seasonal scale (spring: March-April-May; summer: June-July-
- 132 August; autumn: September-October-November; winter: December-January-February). For each season, the $KZ_{(365,3)}$ filter
- was applied to extract the long-term trends in observed, meteorology-driven, and emission-driven MDA8 O₃ concentrations
- 134 (see details in Fig. S1) during 2013–2022, as detailed in Sections 2.2.2, 2.2.3, and 2.2.4.

135 2.2.2 Stepwise MLR for separating meteorological influence

- 136 As vividly illustrated in Fig. S1, a data-based TSM (i.e., MLR integrating the KZ filter) was employed to separate the observed
- 137 MDA8 O₃ concentrations into meteorology-driven and emission-driven concentrations (Sadeghi et al., 2022; Shang et al., 2023;
- 2 Zhang et al., 2022a). We initially applied the KZ filter to disassemble the MDA8 O₃ time series and all meteorological variables

- 139 listed in Table S2 into short-term, baseline, and long-term components at individual state-controlled stations for each season.
- 140 Subsequently, a series of screening processes aligned with our previous research (Wang et al., 2024c), were executed to
- 141 perform stepwise MLR on the short-term/baseline MDA8 O₃ concentrations and a group of meteorological variables series,
- respectively. The established MLR model is presented herein:

$$C_{s,r}(t) = b_{0,s,r} + \sum_{i=1}^{k} b_{i,s,r} \times Met_i(t) + \varepsilon$$
(5)

- Here, $C_{s,r}(t)$ represents the MDA8 O₃ concentration for season s and monitoring station r, while $Met_i(t)$ signifies the i-th
- meteorological variable out of a total of k, and $b_{i,s,r}$ is the corresponding regression coefficient. $b_{0,s,r}$ denotes the intercept
- 145 term, and ε is the residual term. After establishing MLR models for the short-term and baseline components in each season,
- we obtain their respective residual terms. The total residuals, which represent the sum of residuals from baseline variables and
- 147 short-term variables, primarily reflect anthropogenic influences. We then applied a $KZ_{(365.3)}$ filter to these aggregated
- residuals to derive long-term emission-driven and meteorology-driven O₃ variations. Finally, the meteorology-driven O₃ trends
- and emission-driven O₃ trends were obtained through Least Square Method.
- 150 The constructed MLR models driven by meteorological variables from ERA5, MERRA2, or FNL in each season will allow a
- 151 comprehensive analysis of multi-dataset uncertainties. The meteorological impact on O₃ trends derived from the MERRA2-
- driven MLR model will also be integrated into the analysis of multi-method uncertainties to improve the comparability of
- 153 results.

154

2.2.3 Random forest (RF) for deriving meteorological influence

- 155 The application of MLM in O₃ air quality research is becoming increasingly prevalent due to its superior accuracy, user-
- friendly nature, and capability to capture nonlinear relationships (Ni et al., 2024; Yao et al., 2024; Zhang et al., 2022b).
- 157 Considering the limited influence of discrepancy in O₃-Meteorology analyses stemming from different machine learning
- algorithms (Wang et al., 2024a), we opted to build a representative MLM known as the meteorological normalisation model
- based on the RF algorithm (Ding et al., 2023; Ji et al., 2024; Zhang et al., 2023), to delineate meteorology- and emission-
- 160 driven O₃ concentrations.
- 161 RF stands out as a tree-based ensemble learning algorithm adept at handling nonlinear issues and reducing overfitting (Breiman,
- 162 2001). An RF model was developed for each state-controlled station in each season to predict the MDA8 O₃ concentration
- using the Python package "Sklearn-RandomForestRegressor". The predictors included six temporal variables (year, month of
- a year, day of a week, day of a month, day of a year, Unix time), serving as proxies for anthropogenic emission intensity
- 165 (Grange et al., 2018), alongside six MERRA2 meteorological variables as listed in Table S2 (i.e. SLP, T2max, U10, V10,
- RH2, PBLHday). The training dataset comprised 70% of the data, while the remaining 30% was reserved for model evaluation.
- 167 A statistical cross-validation technique was employed to determine optimal hyperparameters for enhancing RF prediction
- 168 performance (Weng et al., 2022). Coefficient of determination (R²) values were utilised to assess model performance for each

station. Over 70% of state-controlled stations showed $R^2 \ge 0.5$ in all seasons (**Fig. S2b**), which is consistent with the 0.4–0.6 range reported in comparable studies (Weng et al., 2022; Lu et al., 2024). Stations with $R^2 < 0.5$ were excluded to avoid significant attribution uncertainty that could be introduced by the RF performance. To evaluate the robustness of the $R^2 \ge 0.5$ criterion, we performed sensitivity analyses using thresholds of $R^2 \ge 0.6$ and $R^2 \ge 0.4$, to ensure that our conclusions are not an artifact of an arbitrary cutoff (**Table S3**).

After establishing the RF model, both the original time variables and resampled meteorological variables were utilised as input data. For meteorological normalisation, we implemented the protocol of Vu et al. (2019). Meteorological variables were resampled by randomly selecting data from the two weeks before and after the specified date, while temporal proxies remained fixed. To derive the de-weathered MDA8 O_3 concentration for a given day (e.g. March 1, 2013), the random resampling process was iterated 1000 times. The mean predicted O_3 under average meteorological conditions, which refers to de-weathered O_3 , corresponds to the emission-driven O_3 concentration. The meteorology-driven MDA8 O_3 concentrations for each season were computed as the difference between observed concentrations and de-weathered concentrations. Detailed processes were are shown in Fig. S2(a). The $KZ_{(365,3)}$ filter was then applied to obtain long-term components, and meteorology-driven O_3 trends were derived using Least Square Method.

2.2.4 GEOS-Chem (GC) simulation for quantifying meteorological influence

The numerical analysis of surface O₃ in China was performed with the GC classic version 13.3.3 (https://github.com/geoschem/GCClassic/releases/tag/13.3.3). Developed as a global 3-D model, GC incorporates a fully coupled O₃–NOx–VOCs–aerosol–halogen chemical mechanism, driven by the MERRA2 meteorological input. Numerous studies have leveraged GC to simulate O₃ air quality in China, demonstrating alignment between observational data and model outcomes (Dai et al., 2024; Dang et al., 2021; Li et al., 2019; Lu et al., 2019a). We employed the nested-grid GC to simulate the long-term surface O₃ concentrations and to quantify the meteorology-driven MDA8 O₃ trends over China. The nested-grid domain was set over China's mainland (15–55°N, 70–140°E) with a horizontal resolution of 0.5° latitude by 0.625° longitude and 47 vertical layers extending up to an altitude of 0.01 hPa. A global simulation with a horizontal resolution of 2°×2.5° provided the chemical boundary conditions for the nested-grid simulation every 3 hours. To ensure model stability and accuracy, a 6-month spin-up simulation was conducted before the commencement of the targeted 10-year period from March 2013 to February 2023.

Emissions management within GC is facilitated by the Harmonized Emissions Component, a system introduced by (Lin et al., 2021b). Anthropogenic emissions are sourced from the Community Emissions Data System (CEDS) inventory globally, with specific overwriting by the Multi-resolution Emission Inventory for China (MEIC) within the Chinese region. The simulations for 2021–2022 adopt a similar approach to Zhai et al. (2021), using 2019 MEIC emissions with NOx emissions reduced by 8 ~ 13% and 2017 MEIC with VOCs emissions reduced by 10 ~ 14%, based on the policy released by Ministry of Ecology and

Environment of the People's Republic of China. For natural emissions, biogenic VOCs, soil, and lightning NOx were calculated online in the model. Emissions from biomass burning, ships, and aircraft are sourced from the Global Fire Emissions Database, the CEDS inventory, and the 2019 Aircraft Emissions Inventory Code, respectively.

203 In order to assess the model's performance and to get a quantification of meteorology-driven O₃ trends during the period of 204 2013-2022, two sets of simulations were conducted: (1) BASE: the standard simulation of O₃ concentrations from 2013 to 205 2022, where both meteorological fields and emissions (including anthropogenic, natural, and biomass emissions) vary year by 206 year from 2013 to 2022; (2) FixE2013: a "fixed-emission simulation" where meteorological conditions vary from 2013 to 207 2022 while anthropogenic emissions remain constant at 2013 levels. The FixE2013 simulation is designed to quantify the 208 meteorological influence on O₃ variations. The FixE2013 simulation is designed to obtain the MDA8 O₃ concentrations driven 209 solely by meteorological changes and further quantify the meteorological influence on O₃ variations in four seasons. After applying the $KZ_{(365.3)}$ filter to derive the long-term meteorology-driven series, trends were calculated through Least Square 210 Method. Figure S3 evaluates the performance of the GC simulation for 2013–2022. The GC model generally captures the 211 212 monthly variability in MDA8 O₃ over China and three eluster-megacity clustersties, with the correlation coefficients greater 213 than 0.80, although it always shows a high bias of surface O_3 in warm seasons (Dai et al., 2024), which can be attributed to its 214 inability to capture the complex terrain, local pollution sources and meteorological conditions, or overestimates of the 215 correlations between the surface O₃ concentration and temperature (Shen et al., 2022; Sun et al., 2021).

2.3 Assessment of uncertainties caused by multi-dataset and multi-method

216

217 In this study, the coefficient of variation (CV) is applied to assess the uncertainties in O₃-Meteorology analyses caused by 218 different meteorological datasets or methods. The CV, calculated as the ratio of the standard deviation (SD) to the mean, serves 219 as a statistical metric commonly utilised to measure the diversity within datasets or models (Bedeian and Mossholder, 2000; 220 Chen et al., 2019). Compared to other comparators (e.g. range, inter-quartile range, and SD), the CV is a unit-free measure 221 that quantifies percentage variation relative to the mean and is less sensitive to outliers and heavy-tailed distributions (Högel 222 et al., 1994; Chattamvelli and Shanmugam, 2023). In this study, higher CVs indicate lower consistency of meteorologically 223 driven O₃ trends derived from different datasets or methods. To give a more quantitative assessment, consistency levels were 224 classified as strong and weak with CV<0.5 and CV>1.0, respectively (Wang et al., 2022a). Given the possibility of disparate 225 meteorology-driven O₃ trends detected by different datasets or methods, we consider the absolute value of the CV as a 226 quantitative indicator of the uncertainties. For each season, when examining the uncertainties arising from different datasets, 227 the CV represents the SD of trends derived from the ERA5, MERRA2, and FNL-driven MLR models divided by the mean. 228 Similarly, in the context of multi-method uncertainties, the CV is the SD of trends identified by the MLR, RF, and GC models 229 divided by the mean.

230 3 Results

231

3.1 Observed trends in surface O₃ concentration

- 232 Figure 2 shows the trends in observed MDA8 O₃ concentrations over a 10-year period during four seasons. Noteworthy
- 233 increases in O_3 concentrations were observed at $78 \sim 93\%$ of state-controlled stations over the years, with the national trend
- being +1.31 ppb yr⁻¹, +0.93 ppb yr⁻¹, +0.79 ppb yr⁻¹, and +0.80 ppb yr⁻¹ in spring, summer, autumn, and winter, respectively.
- 235 The major eastern megacity clusters in China also displayed their highest MDA8 O₃ increase trends in spring, with trends of
- +1.16 ppb yr⁻¹ in BTH, +1.61 ppb yr⁻¹ in YRD, and +1.48 ppb yr⁻¹ in PRD, which has been reported in previous studies (Cao
- et al., 2024b; Chen et al., 2020; Wang et al., 2022b). During summer, BTH and YRD faced more severe challenges in O₃
- 238 prevention and control compared to PRD, with rising MDA8 O₃ trends in the former two regions being about three times
- 239 higher than that in PRD (Fig. 2b).
- 240 In terms of O₃ growth rates, Shanxi province and Anhui province ranked the top two provinces in China over the past decade
- 241 in all seasons except for winter, consistent with Zhao et al. (2020). In spring and winter, O₃ concentrations increased in all
- 242 provinces, with trends of $\pm 0.39 \sim \pm 2.75$ ppb yr⁻¹ and $\pm 0.42 \sim \pm 1.30$ ppb yr⁻¹, respectively. Notably, Jilin province experienced
- 243 an obvious improvement in O_3 air quality during summer and autumn, with decreasing trends of -0.74 ppb yr⁻¹ and -0.38 ppb
- 244 yr⁻¹, respectively, which was also confirmed by Gong et al. (2022). As mentioned in Section 1, variations in O₃ concentrations
- 245 are fundamentally modulated by emissions and meteorology. This section mainly documents observed O₃ trends, and the
- quantitative contributions of emissions and meteorology to MDA8 O₃ variations will be discussed in Section 3.2.
- 247 The annual and seasonal mean MDA8 O₃ concentrations across China are detailed in Fig. S4 and Fig. S5, providing a holistic
- 248 depiction of the persisting spread of O₃ pollution since 2013. On a national average, the O₃ air quality was worst in summer,
- 249 with the average O₃ levels exceeding the air quality standard Grade I limit of 50 ppb almost every year. Notably, the summer
- 250 of 2019 marked a peak period for O₃ pollution, with an average concentration of 59.7 ppb (Fig. S5b).

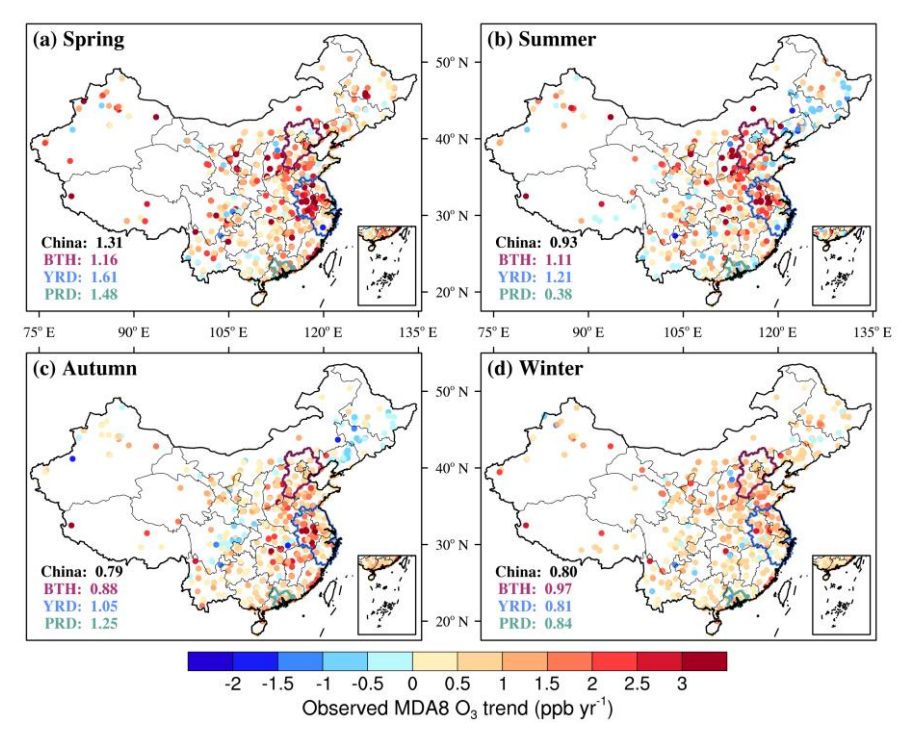


Figure 2. Trends in observed MDA8 O₃ concentrations in China from 2013 to 2022 during (a) spring, (b) summer, (c) autumn, and (d) winter. Values in black, purple, blue, and green represent the mean trends for the whole China, BTH, YRD, and PRD, respectively.

3.2 Uncertainty in meteorology-driven O₃ trends caused by multi-dataset

The traditional statistical method (the MLR model), which has a relatively low computational cost but can provide valuable insights into the quantification of meteorological contributions to O₃ trends, was used to investigate the uncertainties in O₃-Meteorology analyses caused by different meteorological datasets. As shown in Fig. 3(a), meteorological conditions contribute to an increase in MDA8 O₃ concentrations across all seasons in China, with the multi-dataset mean trends ranging from +0.19 (±0.47) ppb yr⁻¹ to +0.55 (±0.45) ppb yr⁻¹. All three dataset-driven MLR models indicate that meteorology leads to the most rapid increase in MDA8 O₃ concentrations in spring, with trends ranging from +0.47 (±0.47) ppb yr⁻¹ to +0.71 (±0.59) ppb yr⁻¹, and a low CV of 0.25. This suggests a high consistency among the three datasets in assessing the meteorological influence on surface O₃ concentrations. During summer and autumn, meteorological influences on O₃ show the—greater spatial heterogeneity (with higher SD) and larger variability among multi-datasets (with higher CV). Specifically in autumn, the meteorology-driven O₃ trend derived from the FNL-driven MLR model is 4.1 times larger than that derived from the ERA5-driven MLR model. Lu et al. (2024) compared meteorology-driven O₃ trends derived from ERA5- and MERRA2-driven MLR models during the summers of 2013–2019. Their findings revealed that ERA5-derived trends were lower than those from MERRA2 in YRD and PRD, whereas trends derived from ERA5 were comparable to those from MERRA2 in BTH. This interstudy consensus further validates the robustness of our methodological framework.

Figure 3(b-d) depicts the meteorological impact on the MDA8 O₃ trends in the three megacity clusters (BTH, YRD, and PRD). Meteorology caused the MDA8 O₃ increase in most of the megacity clusters and seasons, except for BTH during autumn. In seasons where the meteorological effects derived from the three MLR models are all positive, the multi-dataset mean trends ranged from $+0.09 \pm 0.38 \pm 0.33 \pm 0.33$

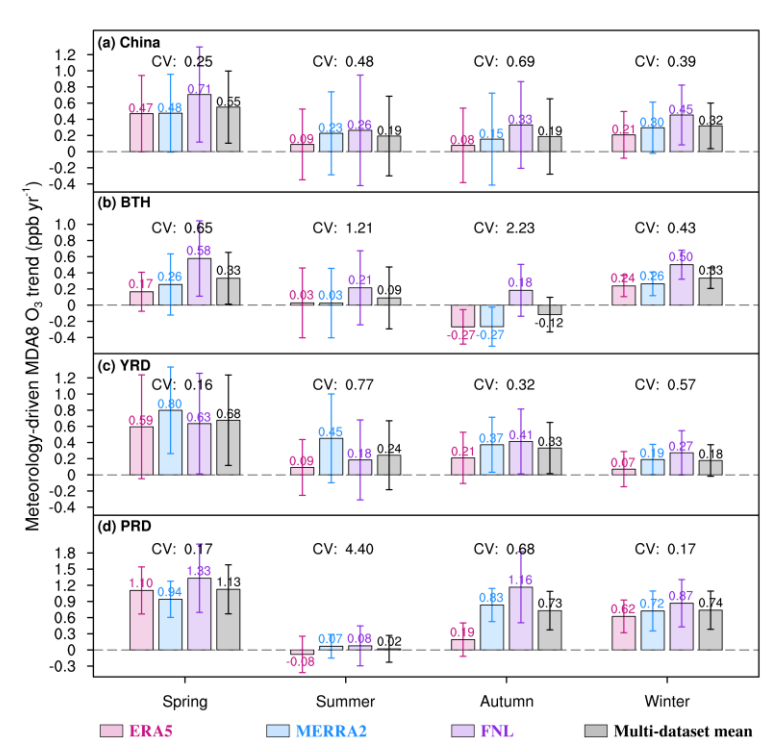


Figure 3. Meteorology-driven MDA8 O₃ trends in (a) the whole China, (b) BTH, (c) YRD, and (d) PRD during four seasons. Values in red, blue, and purple represent trends calculated by ERA5-, MERRA2-, and FNL-driven multiple linear regression (MLR) models, respectively. The fourth black bar represents the multi-dataset mean trend. Error bars indicate ±1 standard deviation (SD) of site-level trends calculated from all available monitoring stations within each region. The absolute value of the coefficient of variation (CV) for each season is also shown.

From a provincial perspective in **Fig. S6**, we can also see that the meteorological contributions to O₃ trends are positive during spring and winter. Large uncertainties in O₃-Meteorology analyses were identified during summer and autumn. There were 7 and 12 provinces with controversial meteorological contributions identified by the three dataset-driven MLR models in summer and autumn, respectively.

Figure 4 displays the spatial distribution of the CV values from the perspective of state-controlled stations in four seasons. Consistent with the national and provincial perspectives, the least uncertainties in O_3 -Meteorology analyses were observed in spring, with CVs less than 0.5 at 45% of stations. Obvious discrepancies in meteorology-driven O_3 trends are found in summer and autumn, particularly in the NCP and northwestern China, with CVs greater than 1.0 at 33 ~ 40% of the stations. In autumn, it is noteworthy that the uncertainties caused by multi-dataset are lower in the south than in the north. Previous studies that employed MLR models to predict O_3 concentration also revealed that the MLR had better performance in the south than in the north (Han et al., 2020; Lu et al., 2024).

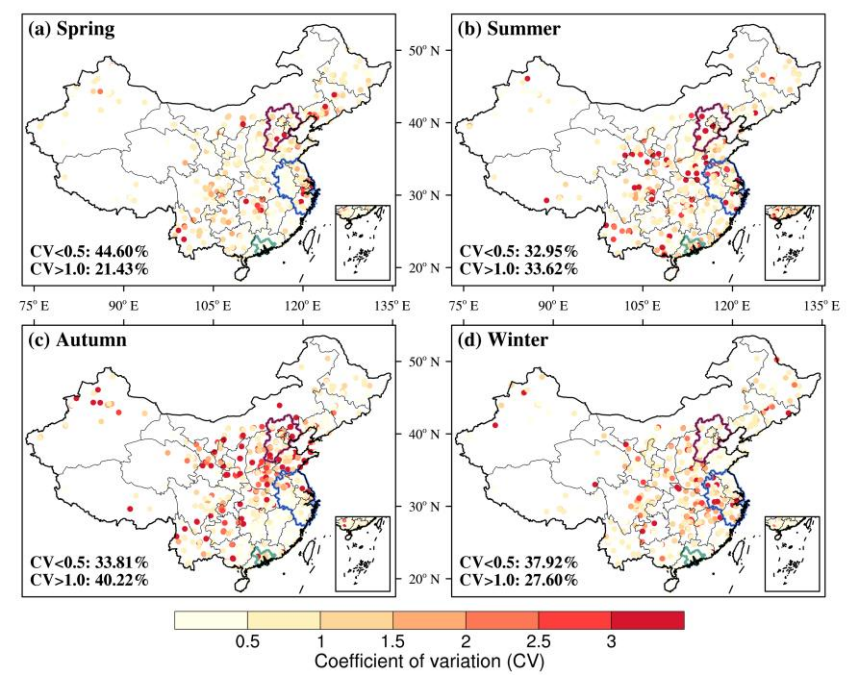


Figure 4. The absolute value of the coefficient of variation (CV) for each state-controlled monitoring station in China during (a) spring, (b) summer, (c) autumn, and (d) winter. The CV is calculated by the standard deviation (SD) of the trends derived from ERA5-, MERRA2-, and FNL-driven MLR models divided by the mean. The darker colour means the larger uncertainty in quantifying the meteorological impact on observed O₃ trends. The proportion of state-control stations with CV less than 0.5 and greater than 1.0 is also shown. The outline marked in purple, blue, and green represents the region of BTH, YRD, and PRD, respectively.

Based on the three dataset-driven MLR models, the meteorological and anthropogenic contributions to the MDA8 O₃ trends in China during 2013–2022 were further examined. As presented in **Fig. 5**, both meteorological conditions and anthropogenic

emissions lead to O₃ increases. According to the ERA5- and MERRA2-driven MLR models, variations in anthropogenic emissions were identified as the dominant factor driving the increase in MDA8 O₃ concentrations across all seasons, with anthropogenic contributions ranging from 63.2% to 90.4%. The results suggest that more stringent emission control policies should be implemented to counteract the adverse effects of meteorological influences on O₃ concentrations.

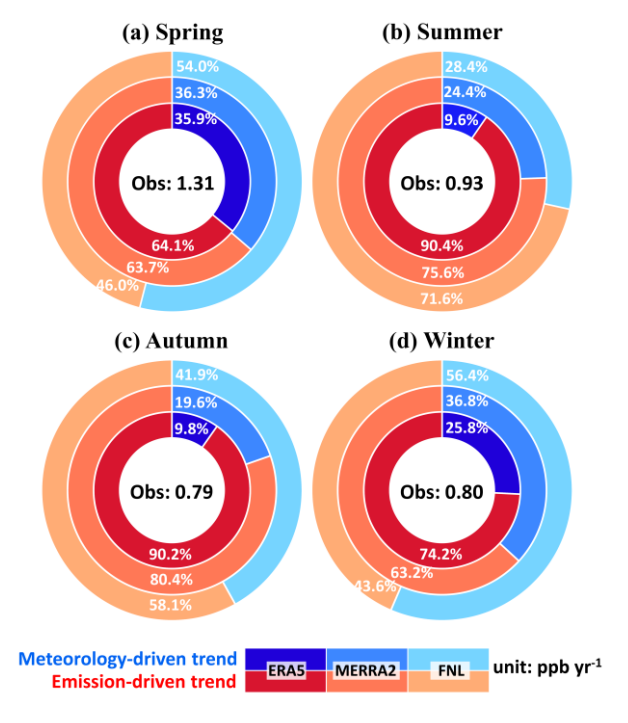


Figure 5. Percentage contributions of meteorological conditions (blue) and anthropogenic emissions (red) to the trends in observed MDA8 O₃ concentrations calculated by ERA5-, MERRA2-, and FNL-driven multiple linear regression (MLR) models in China during (a) spring, (b) summer, (c) autumn, and (d) winter. Values in black represent the observed MDA8 O₃ trends averaged over the whole China.

It is interesting to note that the FNL-driven model almost always gave relatively larger predictions of meteorologically driven O₃ trends compared to the models driven by ERA5 and MERRA2. To investigate whether this discrepancy was due to the coarser spatial resolution of the FNL dataset, a comparison was made between the FNL025-driven MLR model (0.25°×0.25°) and the FNL-driven MLR model (1.0°×1.0°). As depicted in **Fig. S7**, the deviation of the meteorology-driven trends calculated by the two MLR models was less than 0.1 in China and three megacity clusters across four seasons, indicating that different spatial resolutions have little effect on O₃-Meteorology analyses. Further examination was conducted to assess the influence of meteorological variables on O₃-Meteorology analyses. **Table S3-S4** lists the 10-year trends in each meteorological factor and shows a great discrepancy in the variable "PBLHday". Zuo et al. (2023) also reported that FNL exhibited the highest uncertainty for the evaluation of PBLH compared to ERA5 and MERRA2, and that its performance may be constrained by complex underlying terrain and static instability (Guo et al., 2021). As **Fig. S8** shows, constructing the FNL-driven MLR

models using six meteorological variables without "PBLHday" can reduce the estimated meteorological impact by 0.08 to 0.20 ppb yr⁻¹. To obtain a more reliable estimate, it is recommended to use MERRA2 reanalysis dataset due to its eclectic result (**Fig. 3**) and avoid using FNL because of the uncertainty brought by PBLH when separating meteorological and anthropogenic influences on O₃ concentrations in China.

3.3 Uncertainty in meteorology-driven O₃ trends caused by multi-method

This section discusses the uncertainties caused by multi-method (i.e. MLR, RF, GC), all of which are driven by the MERRA2 dataset. **Figure 6** illustrates the meteorology-driven MDA8 O_3 trends calculated by the MLR, RF, and GC models. For the whole of China, the large uncertainties were are evident during summer, when the meteorology-driven O_3 trends derived from the MLR model are notably larger than those from the RF and GC models, with a CV of $2.0\underline{0}$ (**Fig. 6a**). In the other three seasons, the multi-method mean trends, ranging from +0.17 (± 0.37) to +0.26 (± 0.27) ppb yr⁻¹, are 1.1 to 2.1 times lower than those computed by the three dataset-driven MLR models (**Fig. 3a**), all models converge on the conclusion that meteorological conditions contribute to the deterioration of O_3 air quality. Meteorology-driven MDA8 O_3 trends exhibited minor variations across different R² thresholds (**Table S3**), indicating that the trends are not an artifact of an arbitrary cutoff.

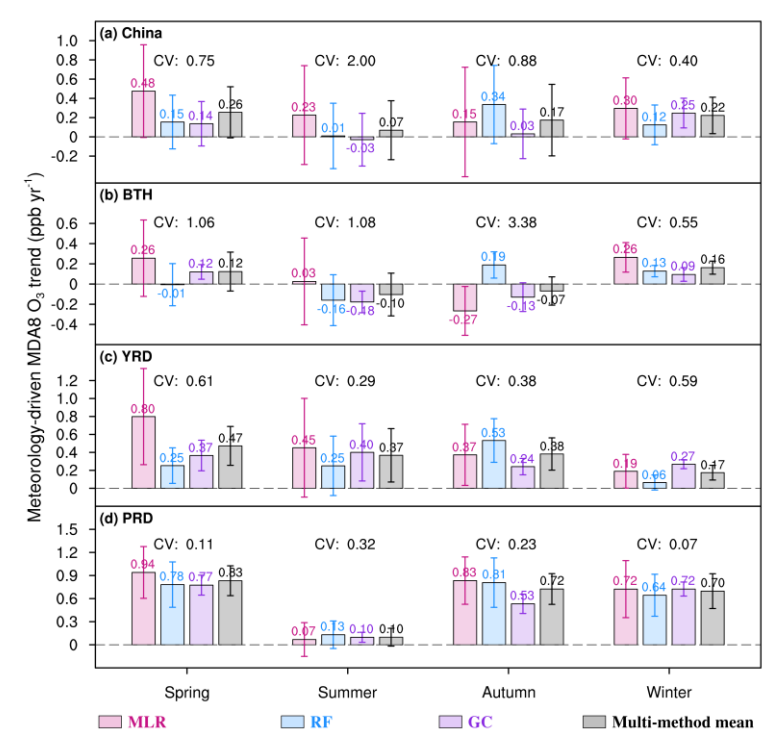


Figure 6. Meteorology-driven MDA8 O₃ trends in (a) the whole China, (b) BTH, (c) YRD, and (d) PRD during four seasons. Values in red, blue, and purple represent trends calculated by multiple linear regression (MLR), random forest (RF), and GEOS-Chem (GC) models, respectively. The fourth black bar represents the multi-method mean trend. Error bars indicate ±1 standard deviation (SD) of site-level trends

calculated from all available monitoring stations within each region. The absolute value of the coefficient of variation (CV) for each season is also shown.

In YRD and PRD, the three models exhibit strong agreement inacross all seasons, with the largesta maximum CV of $0.61_{7.2}$ The low uncertainties are further corroborated by consistent CV estimates derived under different RF's R² thresholds (Table S3). Across these regions, where meteorology leads to an increase in O₃ concentrations with multi-method mean trends of $+0.17 (\pm 0.08)$ to $+0.47 (\pm 0.22)$ ppb yr⁻¹ in YRD and $+0.10 (\pm 0.12)$ to $+0.83 (\pm 0.19)$ ppb yr⁻¹ in PRD, respectively. Notably, the most rapid meteorology-driven O₃ increase is also observed in spring (Fig. 6c and Fig. 6d), which is consistent with Fig. 3c and Fig. 3d. Lu et al. (2024) also demonstrated a high degree of consistency among the MLR, ML, and GC models in PRD during summer. Specifically, all three models indicated that meteorology contributed approximately 25% of O₃ variability over the period 2013–2019. In BTH, the three models perform consistently well only in winter, with meteorology-driven O₃ trends ranging from $+0.09 (\pm 0.07)$ to $+0.26 (\pm 0.15)$ ppb yr⁻¹ and a CV of 0.55. It is also observed that in summer and autumn, meteorology plays a relatively small role in influencing O₃ air quality despite the controversial results obtained by the three models (Fig. 6b). This finding aligns with a study focusing on the O₃ air quality in BTH from 2015 to 2022 (Luo et al., 2024), which suggested that meteorological conditions tend to increase MDA8 O₃ concentration by only 0.01 µg m⁻³ in summer and decrease MDA8 O₃ concentration by 0.3 µg m⁻³ in autumn from 2015 to 2022.

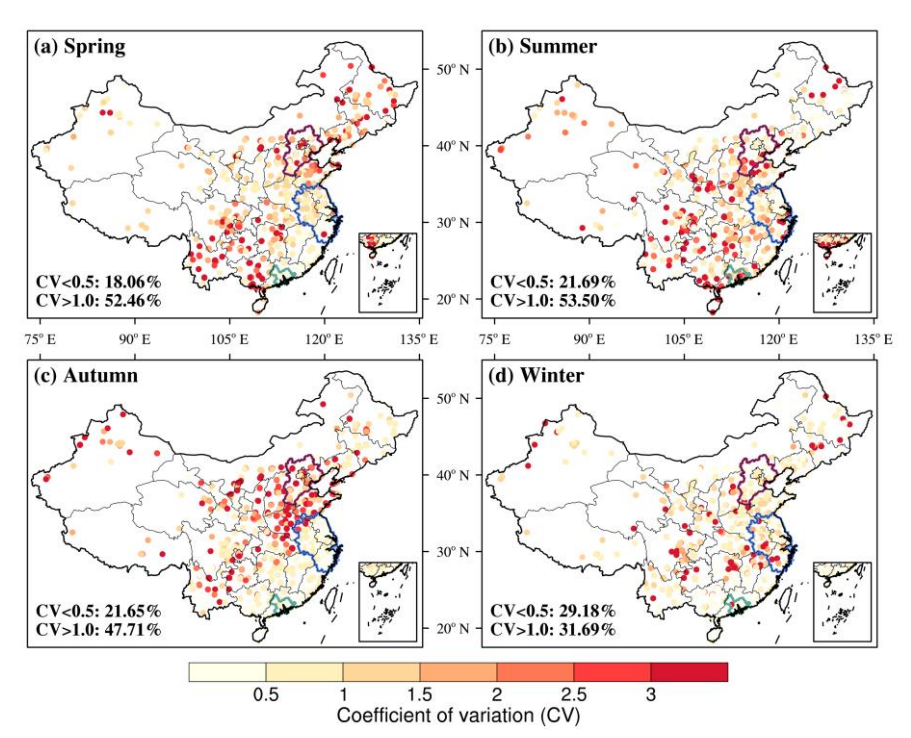


Figure 7. The absolute value of the coefficient of variation (CV) for each state-controlled monitoring station in China during (a) spring, (b) summer, (c) autumn, and (d) winter. The CV is calculated by the standard deviation (SD) of the trends derived from multiple linear regression

359 (MLR), random forest (RF), and GEOS-Chem (GC) models divided by the mean. The darker colour means the larger uncertainty in 360 quantifying the meteorological impact on observed O₃ trends. The proportion of state-control stations with CV less than 0.5 and greater than

361 1.0 is also presented. The outline marked in purple, blue, and green represents the region of BTH, YRD, and PRD, respectively.

362 In addition, Fig. 6 illustrates that the meteorology-driven O₃ trends obtained from GC are relatively smaller. As shown in Fig. S3 and Table S4S5, this difference could partly be attributed to the higher O₃ levels and lower O₃ increases simulated by the GC model before 2018. The GC's systematic overestimation of O₃ concentrations, as well as underestimation of O₃ increases, 364

were-was also reported by Lu et al. (2024), in which the GC captured 13.6 ~ 81.1% of the observed O₃ increases in China

366 during the summer of 2000–2019. It is crucial to take into account the overestimation of low-level O₃ observations, as noted

in previous studies (Hu et al., 2024c; Mao et al., 2024). To validate this hypothesis, we compared the meteorology-driven O₃

trends calculated by MLR with those calculated by GC from 2018 to 2022, and a higher agreement was found over 2018–2022

compared to the 2013-2022 period in Fig. S9. The trends driven by RF model are eclectic in more cases (Fig. 6) and

recommended to isolate meteorological and anthropogenic drivers.

371 From a provincial perspective, as depicted in Fig. S10, the three models together indicate that meteorology causes an O₃

increase in winter across almost all provinces except for Guizhou and Sichuan. In summer and autumn, meteorology leads to

a decrease in 5 provinces, mainly in northeastern China, with trends ranging from -0.42 to -0.11 ppb yr⁻¹. Interestingly, across

all seasons, the three models introduce less uncertainty in the developed east coast regions such as Jiangsu, Fujian, and

375 Guangdong compared to other provinces. This suggests that quantifying meteorological impact on O₃ levels in these developed

376 regions along the east coast of China is relatively reliable.

377 From the perspective of state-controlled stations, Fig. 7 shows the spatial distribution of the CV during four seasons. The

378 lowest disparities in the meteorology-driven MDA8 O₃ trends persist in winter, with CVs of less than 0.5 recorded at 29% of

the stations. In the other three seasons, however, significant discrepancies in meteorology-driven O₃ trends are prominent, with

380 a-CVs greater than 1.0 at least 48% of the stations. Similar to Fig. 4, it is noteworthy that in autumn, the uncertainties caused

381 by multi-method are more pronounced in the northern regions compared to the southern regions.

4 Limitations

363

365

367

368

369

370

372 373

374

379

382

- 383 While this study advances understanding of meteorological contributions to O₃ trends, several limitations warrant attention in
- 384 future work. Though the reanalysis meteorological dataset is generated observationally, inherent constraints exist, including
- 385 parameterization uncertainties affecting O₃-relevant physical processes (Janjić et al., 2018; Davidson and Millstein, 2022) and
- 386 resolution constraints.
- 387 Regarding analytical approaches, machine learning efficiently captures nonlinear O₃-meteorology relationships without
- 388 requiring explicit physicochemical parameterizations, enabling scalable multi-site analysis. However, its inability to resolve

- chemical mechanisms and sensitivity to predictor selection remain key constraints. Conversely, while <u>GEOS-ChemGC</u> mechanistically resolves chemistry-transport interactions and enables source attribution, it propagates uncertainties from emission inventories and chemical mechanisms into trend estimates.
- Future studies could be improved in the following ways: First, more meteorological datasets and methods should be used to provide more robust uncertainty quantification in O₃-meteorology analyses. Second, implementing clustering techniques (e.g.
- 394 K-means algorithm) could identify sub-regional drivers at ecotones, enhancing spatial resolution beyond our regional
- 395 framework. Finally, the Lindeman-Merenda-Gold indices can be employed to quantitatively resolve the contributions of
- 396 specific meteorological variables. The mechanistic understanding of O₃ drivers would be improved by integrating additional
- 397 variables, such as solar radiation, soil moisture, and climate indices (e.g. El Niño-Southern Oscillation). Clustering techniques
- 398 would be valuable to augment the region-based approach and would provide better understanding of the similarity between
- 399 stations.

400

5 Conclusions and Discussions

- 401 This study used the 10-year (2013–2022) surface O₃ observations to clarify O₃ variations during four seasons in China, and
- 402 quantify the meteorological impacts on O₃ trends, with a special focus on the uncertainties of meteorology-driven O₃ trends.
- 403 Diverse meteorological datasets (ERA5, MERRA2, FNL) and analytical methods (MLR, RF, GEOS-Chem) were employed
- 404 to systematically analyse the uncertainties in meteorology-driven O₃ trends caused by multi-dataset and multi-method which
- 405 have not been assessed before. The coefficient of variation (CV) was adopted as a metric to assess the uncertainty. The main
- 406 conclusions are as follows:
- 407 Over the past decade, increasing trends in MDA8 O₃ were observed at over 78% of state-controlled stations across all seasons,
- 408 with the national trend of +1.31 ppb yr⁻¹, +0.93 ppb yr⁻¹, +0.79 ppb yr⁻¹, and +0.80 ppb yr⁻¹ in spring, summer, autumn, and
- 409 winter, respectively.
- 410 We first applied the MLR model (driven by ERA5, MERRA2, and FNL, respectively), which has proven its usefulness and
- 411 reliability in O₃-Meteorology analyses, to assess uncertainties caused by multi-dataset. For the whole China, all three dataset-
- 412 driven MLR models indicate that meteorological conditions have led to an increase in MDA8 O₃ concentrations in four seasons,
- with multi-dataset mean trends ranging from +0.19 ppb yr⁻¹ to +0.55 ppb yr⁻¹. The models driven by different meteorological
- datasets showed a maximum meteorology-driven O₃ trend of +0.55 ppb yr⁻¹ with the highest consistency (CV=0.25) in spring.
- 415 The FNL-driven model always obtained larger meteorology-driven O₃ trends compared to the models driven by ERA5 and
- 416 MERRA2, which could be attributed to the inability to accurately evaluate PBLH in the FNL dataset. The dominant influence
- 417 of anthropogenic emissions on O₃ increase was also identified, highlighting the need for more stringent emission control
- 418 policies to mitigate the adverse effects of meteorological conditions.

- 419 We further applied the MLR, RF, and GEOS-Chem models to obtain the meteorological influence on O₃ trends to explore the 420 uncertainties caused by multi-method. In China and three megacity clusters, the three methods consistently indicated positive 421 meteorological contributions to O₃ increases during spring and winter, with multi-method mean trends ranging from +0.12 to +0.83 ppb yr⁻¹ and +0.17 to +0.70 ppb yr⁻¹, respectively. In summer and autumn, especially in BTH, where the meteorological 422 423 influence was relatively lower, three methods gave conflicting predictions of meteorological influence on O₃ with CVs greater 424 than 1.08. For the whole China, three different methods demonstrated optimal consistency in winter with a CV of 0.40 and the 425 worst consistency in summer with a CV of 2.00. The meteorology-driven O₃ trends obtained from GEOS-Chem model were 426 almost relatively smaller than those obtained by other two methods, which could partly be attributed to the higher O₃ values 427 simulated by the GEOS-Chem model before 2018.
- All analyses driven by diverse meteorological datasets and analytical methods drew a consistent finding: meteorological conditions almost contribute to O₃ increase across all seasons. The uncertainties of meteorology-driven O₃ trends caused by different analytical methods were larger than those caused by diverse meteorological datasets. Considering that the favourable effects of meteorology on O₃ pollution tend to be weaker after 2019 and the effects of COVID-19, it is necessary to conduct research over different periods and longer periods. In addition, further research is needed to focus on the meteorological contributions to O₃ trends in northern China due to larger uncertainties.
- 434 Data availability. The surface O₃ observations are obtained from https://quotsoft.net/air/. The ERA5, MERRA2, FNL, and 435 FNL025 reanalysis meteorological taken from https://cds.climate.copernicus.eu/datasets, data are http://geoschemdata.wustl.edu/ExtData/GEOS 0.5x0.625 AS/MERRA-2/, https://rda.ucar.edu/datasets/d083002/, 436 437 https://rda.ucar.edu/datasets/ds083-3/, respectively. The code of the GEOS-Chem (version 13.3.3) model is available at 438 https://zenodo.org/records/5748260. The MDA8 O₃ observations and analytical results derived from MLR, RF, and GEOS-439 Chem can be obtained from https://doi.org/10.5281/zenodo.15859027.
- Author contributions. JZ designed the research, and XW performed simulations and analysed the results. GJ, XC, and ZY helped with the model simulations. LC, XJ, and HL provided useful comments on the paper. XW and JZ wrote the paper with contributions from all co-authors.
- 443 **Competing interests.** The authors declare that they have no conflict of interest.
- Financial support. This research has been supported by National Nature Science Foundation of China (No.42293323, 42007195, 42305121), National Key Research and Development Program of China (No.2022YFE0136100), State Environmental Protection Key Laboratory of Sources and Control of Air Pollution Complex (No.SCAPC202114), and Natural
- 447 Science Foundation of Jiangsu Province (No.BK20220031).

448 References

- 449 Bedeian, A. G. and Mossholder, K. W.: On the use of the coefficient of variation as a measure of diversity, Organ. Res.
- 450 Methods, 3, 285–297, https://doi.org/10.1177/109442810033005, 2000.
- 451 Breiman, L.: Random forests, Mach. Learn., 45, 5–32, https://doi.org/10.1023/A:1010933404324, 2001.
- 452 Cao, T., Wang, H., Li, L., Lu, X., Liu, Y., and Fan, S.: Fast spreading of surface ozone in both temporal and spatial scale in
- 453 Pearl River Delta, J. Environ. Sci., 137, 540–552, https://doi.org/10.1016/j.jes.2023.02.025, 2024a.
- 454 Cao, T., Wang, H., Chen, X., Li, L., Lu, X., Lu, K., and Fan, S.: Rapid increase in spring ozone in the Pearl River Delta, China
- during 2013-2022, npj Clim. Atmos. Sci., 7, 309, https://doi.org/10.1038/s41612-024-00847-3, 2024b.
- 456 Chattamvelli, R., Shanmugam, R. Measures of Spread. In: Descriptive Statistics for Scientists and Engineers. Synthesis
- 457 Lectures on Mathematics & Statistics. Springer, Cham. https://doi.org/10.1007/978-3-031-32330-0 3, 2019
- 458 Chen, L., Gao, Y., Zhang, M., Fu, J. S., Zhu, J., Liao, H., Li, J., Huang, K., Ge, B., Wang, X., Lam, Y. F., Lin, C.-Y., Itahashi,
- 459 S., Nagashima, T., Kajino, M., Yamaji, K., Wang, Z., and Kurokawa, J.: MICS-Asia III: multi-model comparison and
- evaluation of aerosol over East Asia, Atmos. Chem. Phys., 19, 11911–11937, https://doi.org/10.5194/acp-19-11911-2019,
- 461 2019.
- 462 Chen, L., Zhu, J., Liao, H., Yang, Y., and Yue, X.: Meteorological influences on PM_{2.5} and O₃ trends and associated health
- burden since China's clean air actions, Sci. Total Environ., 744, 140837, https://doi.org/10.1016/j.scitotenv.2020.140837,
- 464 2020.
- 465 Dai, H., Liao, H., Wang, Y., and Qian, J.: Co-occurrence of ozone and PM_{2.5} pollution in urban/non-urban areas in eastern
- China from 2013 to 2020: roles of meteorology and anthropogenic emissions, Sci. Total Environ., 924, 171687,
- 467 https://doi.org/10.1016/j.scitotenv.2024.171687, 2024.
- 468 Dai, Q., Dai, T., Hou, L., Li, L., Bi, X., Zhang, Y., and Feng, Y.: Quantifying the impacts of emissions and meteorology on
- 469 the interannual variations of air pollutants in major Chinese cities from 2015 to 2021, Sci. China Earth Sci.,
- 470 https://doi.org/10.1007/s11430-022-1128-1, 2023.
- 471 Dang, R., Liao, H., and Fu, Y.: Quantifying the anthropogenic and meteorological influences on summertime surface ozone in
- 472 China over 2012–2017, Sci. Total Environ., 754, 142394, https://doi.org/10.1016/j.scitotenv.2020.142394, 2021.
- 473 Davidson, M. R. and Millstein, D.: Limitations of reanalysis data for wind power applications, Wind Energy, 25, 1646–1653,
- 474 https://doi.org/10.1002/we.2759, 2022.
- 475 Ding, J., Dai, Q., Fan, W., Lu, M., Zhang, Y., Han, S., and Feng, Y.: Impacts of meteorology and precursor emission change
- on O₃ variation in Tianjin, China from 2015 to 2021, J. Environ. Sci., 126, 506-516,
- 477 https://doi.org/10.1016/j.jes.2022.03.010, 2023.
- 478 Eskridge, R. E., Ku, J. Y., Rao, S. T., Porter, P. S., and Zurbenko, I. G.: Separating different scales of motion in time series of
- 479 meteorological variables, Bull. Am. Meteorol. Soc., 78, 1473-1483, https://doi.org/10.1175/1520-
- 480 0477(1997)078<1473:SDSOMI>2.0.CO;2, 1997.

- 481 Gao, M., Wang, F., Ding, Y., Wu, Z., Xu, Y., Lu, X., Wang, Z., Carmichael, G. R., and McElroy, M. B.: Large-scale climate
- 482 patterns offer preseasonal hints on the co-occurrence of heat wave and O₃ pollution in China, Proc. Natl. Acad. Sci., 120,
- 483 e2218274120, https://doi.org/10.1073/pnas.2218274120, 2023.
- 484 Gong, S., Zhang, L., Liu, C., Lu, S., Pan, W., and Zhang, Y.: Multi-scale analysis of the impacts of meteorology and emissions
- on PM_{2.5} and O₃ trends at various regions in China from 2013 to 2020 2. Key weather elements and emissions, Sci. Total
- 486 Environ., 824, 153847, https://doi.org/10.1016/j.scitotenv.2022.153847, 2022.
- 487 Grange, S. K., Carslaw, D. C., Lewis, A. C., Boleti, E., and Hueglin, C.: Random forest meteorological normalisation models
- 488 for Swiss PM₁₀ trend analysis, Atmos. Chem. Phys., 18, 6223–6239, https://doi.org/10.5194/acp-18-6223-2018, 2018.
- 489 Guo, J., Zhang, J., Yang, K., Liao, H., Zhang, S., Huang, K., Lv, Y., Shao, J., Yu, T., Tong, B., Li, J., Su, T., Yim, S. H. L.,
- 490 Stoffelen, A., Zhai, P., and Xu, X.: Investigation of near-global daytime boundary layer height using high-resolution
- 491 radiosondes: first results and comparison with ERA5, MERRA-2, JRA-55, and NCEP-2 reanalyses, Atmos. Chem. Phys.,
- 492 21, 17079–17097, https://doi.org/10.5194/acp-21-17079-2021, 2021.
- 493 Han, H., Liu, J., Shu, L., Wang, T., and Yuan, H.: Local and synoptic meteorological influences on daily variability in
- summertime surface ozone in eastern China, Atmos. Chem. Phys., 20, 203–222, https://doi.org/10.5194/acp-20-203-2020,
- 495 2020.
- 496 He, X., Leng, C., Pang, S., and Zhang, Y.: Kinetics study of heterogeneous reactions of ozone with unsaturated fatty acid
- single droplets using micro-FTIR spectroscopy, RSC Adv., 7, 3204–3213, https://doi.org/10.1039/C6RA25255A, 2017.
- 498 Högel, J., Schmid, W., and Gaus, W.: Robustness of the standard deviation and other measures of dispersion, Biom. J., 36,
- 499 411–427, https://doi.org/10.1002/bimj.4710360403, 1994.
- Hu, F., Xie, P., Xu, J., Lv, Y., Zhang, Z., Zheng, J., and Tian, X.: Long-term trends of ozone in the Yangtze River Delta, China:
- 501 spatiotemporal impacts of meteorological factors, local, and non-local emissions, J. Environ. Sci., S1001074224003826,
- 502 https://doi.org/10.1016/j.ies.2024.07.017, 2024a.
- 503 Hu, T., Lin, Y., Liu, R., Xu, Y., Ouyang, S., Wang, B., Zhang, Y., and Liu, S. C.: What caused large ozone variabilities in
- three megacity clusters in eastern China during 2015-2020?, Atmos. Chem. Phys., 24, 1607-1626,
- 505 https://doi.org/10.5194/acp-24-1607-2024, 2024b.
- 506 Hu, W., Zhao, Y., Lu, N., Wang, X., Zheng, B., Henze, D. K., Zhang, L., Fu, T.-M., and Zhai, S.: Changing Responses of
- 507 PM_{2.5} and Ozone to Source Emissions in the Yangtze River Delta Using the Adjoint Model, Environ. Sci. Technol., 58,
- 508 628–638, https://doi.org/10.1021/acs.est.3c05049, 2024c.
- 509 Janjić, T., Bormann, N., Bocquet, M., Carton, J. A., Cohn, S. E., Dance, S. L., Losa, S. N., Nichols, N. K., Potthast, R., Waller,
- J. A., and Weston, P.: On the representation error in data assimilation, Q. J. R. Meteorolog. Soc., 144, 1257–1278,
- 511 https://doi.org/10.1002/qj.3130, 2018.
- 512 Ji, X., Chen, G., Chen, J., Xu, L., Lin, Z., Zhang, K., Fan, X., Li, M., Zhang, F., Wang, H., Huang, Z., and Hong, Y.:
- 513 Meteorological impacts on the unexpected ozone pollution in coastal cities of China during the unprecedented hot summer
- of 2022, Sci. Total Environ., 914, 170035, https://doi.org/10.1016/j.scitotenv.2024.170035, 2024.

- 515 Li, K., Jacob, D. J., Liao, H., Shen, L., Zhang, Q., and Bates, K. H.: Anthropogenic drivers of 2013-2017 trends in summer
- surface ozone in China, Proc. Natl. Acad. Sci., 116, 422–427, https://doi.org/10.1073/pnas.1812168116, 2019.
- 517 Li, K., Jacob, D. J., Shen, L., Lu, X., De Smedt, I., and Liao, H.: Increases in surface ozone pollution in China from 2013 to
- 518 2019: anthropogenic and meteorological influences, Atmos. Chem. Phys., 20, 11423–11433, https://doi.org/10.5194/acp-
- 519 20-11423-2020, 2020.
- 520 Li, K., Jacob, D. J., Liao, H., Qiu, Y., Shen, L., Zhai, S., Bates, K. H., Sulprizio, M. P., Song, S., Lu, X., Zhang, Q., Zheng,
- B., Zhang, Y., Zhang, J., Lee, H. C., and Kuk, S. K.: Ozone pollution in the north China plain spreading into the late-
- 522 winter haze season, Proc. Natl. Acad. Sci., 118, e2015797118, https://doi.org/10.1073/pnas.2015797118, 2021.
- 523 Li, X., Yuan, B., Parrish, D. D., Chen, D., Song, Y., Yang, S., Liu, Z., and Shao, M.: Long-term trend of ozone in southern
- 524 China reveals future mitigation strategy for air pollution, Atmos. Environ., 269, 118869,
- 525 https://doi.org/10.1016/j.atmosenv.2021.118869, 2022.
- 526 Lin, C., Lau, A. K. H., Fung, J. C. H., Song, Y., Li, Y., Tao, M., Lu, X., Ma, J., and Lao, X. Q.: Removing the effects of
- meteorological factors on changes in nitrogen dioxide and ozone concentrations in China from 2013 to 2020, Sci. Total
- 528 Environ., 793, 148575, https://doi.org/10.1016/j.scitotenv.2021.148575, 2021a.
- 529 Lin, H., Jacob, D. J., Lundgren, E. W., Sulprizio, M. P., Keller, C. A., Fritz, T. M., Eastham, S. D., Emmons, L. K., Campbell,
- P. C., Baker, B., Saylor, R. D., and Montuoro, R.: Harmonized Emissions Component (HEMCO) 3.0 as a versatile
- emissions component for atmospheric models: application in the GEOS-Chem, NASA GEOS, WRF-GC, CESM2, NOAA
- 532 GEFS-Aerosol, and NOAA UFS models, Geosci. Model Dev., 14, 5487–5506, https://doi.org/10.5194/gmd-14-5487-
- 533 2021, 2021b.
- 534 Liu, Y. and Wang, T.: Worsening urban ozone pollution in China from 2013 to 2017 part 1: the complex and varying roles
- of meteorology, Atmos. Chem. Phys., 20, 6305–6321, https://doi.org/10.5194/acp-20-6305-2020, 2020a.
- 536 Liu, Y. and Wang, T.: Worsening urban ozone pollution in China from 2013 to 2017 part 2: the effects of emission changes
- and implications for multi-pollutant control, Atmos. Chem. Phys., 20, 6323–6337, https://doi.org/10.5194/acp-20-6323-
- 538 2020, 2020b.
- 539 Liu, Y., Geng, G., Cheng, J., Liu, Y., Xiao, Q., Liu, L., Shi, Q., Tong, D., He, K., and Zhang, Q.: Drivers of Increasing Ozone
- during the Two Phases of Clean Air Actions in China 2013–2020, Environ. Sci. Technol., 57, 8954–8964,
- 541 https://doi.org/10.1021/acs.est.3c00054, 2023.
- 542 Lu, X., Zhang, L., Chen, Y., Zhou, M., Zheng, B., Li, K., Liu, Y., Lin, J., Fu, T.-M., and Zhang, Q.: Exploring 2016–2017
- surface ozone pollution over China: source contributions and meteorological influences, Atmos. Chem. Phys., 19, 8339–
- 544 8361, https://doi.org/10.5194/acp-19-8339-2019, 2019a.
- 545 Lu, X., Zhang, L., and Shen, L.: Meteorology and Climate Influences on Tropospheric Ozone: a Review of Natural Sources,
- 546 Chemistry, and Transport Patterns, Curr. Pollut. Rep., 5, 238–260, https://doi.org/10.1007/s40726-019-00118-3, 2019b.
- 547 Lu, X., Liu, Y., Su, J., Weng, X., Ansari, T., Zhang, Y., He, G., Zhu, Y., Wang, H., Zeng, G., Li, J., He, C., Li, S.,
- 548 Amnuaylojaroen, T., Butler, T., Fan, Q., Fan, S., Forster, G. L., Gao, M., Hu, J., Kanaya, Y., Latif, M. T., Lu, K., Nédélec,

- P., Nowack, P., Sauvage, B., Xu, X., Zhang, L., Li, K., Koo, J.-H., and Nagashima, T.: Tropospheric ozone trends and
- attributions over east and southeast Asia in 1995–2019: an integrated assessment using statistical methods, machine
- learning models, and multiple chemical transport models, https://doi.org/10.5194/egusphere-2024-3702, 17 December
- 552 2024.
- 553 Luo, Z., Lu, P., Chen, Z., and Liu, R.: Ozone Concentration Estimation and Meteorological Impact Quantification in the
- Beijing-Tianjin-Hebei Region Based on Machine Learning Models, Earth Space Sci., 11, e2023EA003346,
- 555 https://doi.org/10.1029/2023EA003346, 2024.
- 556 Lyu, X., Li, K., Guo, H., Morawska, L., Zhou, B., Zeren, Y., Jiang, F., Chen, C., Goldstein, A. H., Xu, X., Wang, T., Lu, X.,
- Zhu, T., Querol, X., Chatani, S., Latif, M. T., Schuch, D., Sinha, V., Kumar, P., Mullins, B., Seguel, R., Shao, M., Xue,
- L., Wang, N., Chen, J., Gao, J., Chai, F., Simpson, I., Sinha, B., and Blake, D. R.: A synergistic ozone-climate control to
- address emerging ozone pollution challenges, One Earth, 6, 964–977, https://doi.org/10.1016/j.oneear.2023.07.004, 2023.
- 560 Mao, Y., Shang, Y., Liao, H., Cao, H., Ou, Z., and Henze, D. K.: Sensitivities of ozone to its precursors during heavy ozone
- 561 pollution events in the Yangtze River Delta using the adjoint method, Sci. Total Environ., 925, 171585,
- 562 https://doi.org/10.1016/j.scitotenv.2024.171585, 2024.
- 563 Mousavinezhad, S., Choi, Y., Pouyaei, A., Ghahremanloo, M., and Nelson, D. L.: A comprehensive investigation of surface
- ozone pollution in China, 2015–2019: separating the contributions from meteorology and precursor emissions, Atmos.
- Res., 257, 105599, https://doi.org/10.1016/j.atmosres.2021.105599, 2021.
- 566 Ni, Y., Yang, Y., Wang, H., Li, H., Li, M., Wang, P., Li, K., and Liao, H.: Contrasting changes in ozone during 2019–2021
- between eastern and the other regions of China attributed to anthropogenic emissions and meteorological conditions, Sci.
- 568 Total Environ., 908, 168272, https://doi.org/10.1016/j.scitotenv.2023.168272, 2024.
- 569 Pan, W., Gong, S., Lu, K., Zhang, L., Xie, S., Liu, Y., Ke, H., Zhang, X., and Zhang, Y.: Multi-scale analysis of the impacts
- of meteorology and emissions on PM_{2.5} and O₃ trends at various regions in China from 2013 to 2020 3. Mechanism
- assessment of O₃ trends by a model, Sci. Total Environ., 857, 159592, https://doi.org/10.1016/j.scitotenv.2022.159592,
- 572 2023.
- 573 Qi, G., Che, J., and Wang, Z.: Differential effects of urbanization on air pollution: evidences from six air pollutants in mainland
- 574 China, Ecol. Indic., 146, 109924, https://doi.org/10.1016/j.ecolind.2023.109924, 2023.
- 575 Qian, J., Liao, H., Yang, Y., Li, K., Chen, L., and Zhu, J.: Meteorological influences on daily variation and trend of summertime
- surface ozone over years of 2015–2020: Quantification for cities in the Yangtze River Delta, Sci. Total Environ., 834,
- 577 155107, https://doi.org/10.1016/j.scitotenv.2022.155107, 2022.
- 578 Qiao, W., Li, K., Yang, Z., Chen, L., and Liao, H.: Implications of the extremely hot summer of 2022 on urban ozone control
- in China, Atmospheric and Oceanic Science Letters, 17, 100470, https://doi.org/10.1016/j.aosl.2024.100470, 2024.
- 580 Rao, S. T. and Zurbenko, I. G.: Detecting and tracking changes in ozone air quality, Air Waste, 44, 1089-1092.
- 581 https://doi.org/10.1080/10473289.1994.10467303, 1994.

- Ren, J., Guo, F., and Xie, S.: Diagnosing ozone–NO_x–VOC sensitivity and revealing causes of ozone increases in China based
- on 2013–2021 satellite retrievals, Atmos. Chem. Phys., 22, 15035–15047, https://doi.org/10.5194/acp-22-15035-2022,
- 584 2022.
- 585 Sadeghi, B., Ghahremanloo, M., Mousavinezhad, S., Lops, Y., Pouyaei, A., and Choi, Y.: Contributions of meteorology to
- ozone variations: Application of deep learning and the Kolmogorov-Zurbenko filter, Environ. Pollut., 310, 119863,
- 587 https://doi.org/10.1016/j.envpol.2022.119863, 2022.
- 588 Shang, N., Gui, K., Zhao, H., Yao, W., Zhao, H., Zhang, X., Zhang, X., Li, L., Zheng, Y., Wang, Z., Wang, Y., Che, H., and
- Zhang, X.: Decomposition of meteorological and anthropogenic contributions to near-surface ozone trends in Northeast
- 590 China (2013–2021), Atmos. Pollut. Res., 14, 101841, https://doi.org/10.1016/j.apr.2023.101841, 2023.
- 591 Shen, F., Zhang, L., Jiang, L., Tang, M., Gai, X., Chen, M., and Ge, X.: Temporal variations of six ambient criteria air pollutants
- from 2015 to 2018, their spatial distributions, health risks and relationships with socioeconomic factors during 2018 in
- 593 China, Environ, Int., 137, 105556, https://doi.org/10.1016/j.envint.2020.105556, 2020.
- 594 Shen, L., Liu, J., Zhao, T., Xu, X., Han, H., Wang, H., and Shu, Z.: Atmospheric transport drives regional interactions of ozone
- 595 pollution in China, Sci. Total Environ., 830, 154634, https://doi.org/10.1016/j.scitotenv.2022s154634, 2022.
- 596 Sun, Y., Yin, H., Lu, X., Notholt, J., Palm, M., Liu, C., Tian, Y., and Zheng, B.: The drivers and health risks of unexpected
- 597 surface ozone enhancements over the Sichuan Basin, China, in 2020, Atmos. Chem. Phys., 21, 18589–18608,
- 598 https://doi.org/10.5194/acp-21-18589-2021, 2021.
- Teixeira, J., Piepmeier, J. R., Nehrir, A. R., Ao, C. O., Chen, S. S., Clayson, C. A., Fridlind, A. M., Lebsock, M., McCarty, W.,
- Salmun, H., Santanello, J. A., Turner, D. D., Wang, Z., and Zeng, X.: Toward a global planetary boundary layer observing
- system: the NASA PBL incubation study team report, NASA PBL Incubation Study Team, 134 pp, 2021
- 602 Vu, T. V., Shi, Z., Cheng, J., Zhang, Q., He, K., Wang, S., and Harrison, R. M.: Assessing the impact of clean air action on air
- 603 quality trends in Beijing using a machine learning technique, Atmos. Chem. Phys., 19, 11303–11314.
- 604 https://doi.org/10.5194/acp-19-11303-2019, 2019.
- 605 Wang, M., Chen, X., Jiang, Z., He, T.-L., Jones, D., Liu, J., and Shen, Y.: Meteorological and anthropogenic drivers of surface
- ozone change in the North China Plain in 2015–2021, Sci. Total Environ., 906, 167763,
- 607 https://doi.org/10.1016/j.scitotenv.2023.167763, 2024a.
- 608 Wang, P.: China's air pollution policies: progress and challenges, Curr. Opin. Environ. Sci. Health, 19, 100227,
- 609 https://doi.org/10.1016/j.coesh.2020.100227, 2021.
- 610 Wang, T., Li, N., Li, Y., Lin, H., Yao, N., Chen, X., Li Liu, D., Yu, Q., and Feng, H.: Impact of climate variability on grain
- 611 yields of spring and summer maize, Comput. Electron. Agric., 199, 107101,
- https://doi.org/10.1016/j.compag.2022.107101, 2022a.
- Wang, T., Xue, L., Brimblecombe, P., Lam, Y. F., Li, L., and Zhang, L.: Ozone pollution in China: a review of concentrations.
- 614 meteorological influences, chemical precursors, and effects, Sci. Total Environ., 575, 1582–1596,
- 615 https://doi.org/10.1016/j.scitotenv.2016.10.081, 2017.

- Wang, W., Parrish, D. D., Wang, S., Bao, F., Ni, R., Li, X., Yang, S., Wang, H., Cheng, Y., and Su, H.: Long-term trend of
- ozone pollution in China during 2014–2020: distinct seasonal and spatial characteristics and ozone sensitivity, Atmos.
- 618 Chem. Phys., 22, 8935–8949, https://doi.org/10.5194/acp-22-8935-2022, 2022b.
- Wang, X., Jiang, L., Guo, Z., Xie, X., Li, L., Gong, K., and Hu, J.: Influence of meteorological reanalysis field on air quality
- 620 modeling in the Yangtze River Delta, China, Atmos. Environ., 318, 120231,
- 621 https://doi.org/10.1016/j.atmosenv.2023.120231, 2024b.
- 622 Wang, X., Zhu, J., Li, K., Chen, L., Yang, Y., Zhao, Y., Yue, X., Gu, Y., and Liao, H.: Meteorology-driven trends in PM_{2.5}
- 623 concentrations and related health burden over India, Atmos. Res., 308, 107548,
- 624 https://doi.org/10.1016/j.atmosres.2024.107548, -2024c.
- Wang, Y., Zhao, Y., Liu, Y., Jiang, Y., Zheng, B., Xing, J., Liu, Y., Wang, S., and Nielsen, C. P.: Sustained emission reductions
- have restrained the ozone pollution over China, Nat. Geosci., 16, 967–974, https://doi.org/10.1038/s41561-023-01284-2,
- 627 2023.
- 628 Wei, J., Li, Z., Li, K., Dickerson, R. R., Pinker, R. T., Wang, J., Liu, X., Sun, L., Xue, W., and Cribb, M.: Full-coverage
- mapping and spatiotemporal variations of ground-level ozone (O₃) pollution from 2013 to 2020 across China, Remote
- 630 Sens. Environ., 270, 112775, https://doi.org/10.1016/j.rse.2021.112775, 2022.
- Weng, X., Forster, G. L., and Nowack, P.: A machine learning approach to quantify meteorological drivers of ozone pollution
- in China from 2015 to 2019, Atmos. Chem. Phys., 22, 8385–8402, https://doi.org/10.5194/acp-22-8385-2022, 2022.
- Weng, X., Li, J., Forster, G. L., and Nowack, P.: Large modeling uncertainty in projecting decadal surface ozone changes over
- 634 city clusters of China, Geophys. Res. Lett., 50, e2023GL103241, https://doi.org/10.1029/2023GL103241, 2023.
- 635 Wise, E. K. and Comrie, A. C.: Extending the Kolmogorov-Zurbenko Filter: Application to Ozone, Particulate Matter, and
- 636 Meteorological Trends, J. Air Waste Manage. Assoc., 55, 1208–1216, https://doi.org/10.1080/10473289.2005.10464718,
- 637 2005.
- 638 Wu, Y., Li D., Zhang L., and Dai H.: Modeling Study on the Impact of Climate Change on Air Pollution. Acta Scientiarum
- 639 Naturalium Universitatis Pekinensis, 59, 854–870. https://doi.org/10.13209/j.0479-8023.2023.010, 2023.
- 640 Yan, D., Jin, Z., Zhou, Y., Li, M., Zhang, Z., Wang, T., Zhuang, B., Li, S., and Xie, M.: Anthropogenically and
- meteorologically modulated summertime ozone trends and their health implications since China's clean air actions,
- 642 Environ. Pollut., 343, 123234, https://doi.org/10.1016/j.envpol.2023.123234, 2024.
- 643 Yao, T., Ye, H., Wang, Y., Zhang, J., Guo, J., and Li, J.: Kolmogorov-Zurbenko filter coupled with machine learning to reveal
- multiple drivers of surface ozone pollution in China from 2015 to 2022, Sci. Total Environ., 949, 175093,
- 645 https://doi.org/10.1016/j.scitotenv.2024.175093, 2024.
- 646 Yin, H., Lu, X., Sun, Y., Li, K., Gao, M., Zheng, B., and Liu, C.: Unprecedented decline in summertime surface ozone over
- eastern China in 2020 comparably attributable to anthropogenic emission reductions and meteorology, Environ, Res. Lett..
- 648 16, 124069, https://doi.org/10.1088/1748-9326/ac3e22, 2021.

- 649 Zhai, S., Jacob, D. J., Wang, X., Liu, Z., Wen, T., Shah, V., Li, K., Moch, J. M., Bates, K. H., Song, S., Shen, L., Zhang, Y.,
- 650 Luo, G., Yu, F., Sun, Y., Wang, L., Qi, M., Tao, J., Gui, K., Xu, H., Zhang, Q., Zhao, T., Wang, Y., Lee, H. C., Choi, H.,
- and Liao, H.: Control of particulate nitrate air pollution in China, Nat. Geosci., 14, 389-395,
- https://doi.org/10.1038/s41561-021-00726-z, 2021.
- 653 Zhang, L., Wang, L., Liu, B., Tang, G., Liu, B., Li, X., Sun, Y., Li, M., Chen, X., Wang, Y., and Hu, B.: Contrasting effects
- of clean air actions on surface ozone concentrations in different regions over Beijing from May to September 2013–2020,
- 655 Sci. Total Environ., 903, 166182, https://doi.org/10.1016/j.scitotenv.2023.166182, 2023.
- 256 Zhang, Y., Lei, R., Cui, S., Wang, H., Chen, M., and Ge, X.: Spatiotemporal trends and impact factors of PM_{2.5} and O₃ pollution
- in major cities in China during 2015–2020, Chin. Sci. Bull., 67, 2029–2042, https://doi.org/10.1360/TB-2021-0767,
- 658 2022a.
- Zhang, Z., Xu, B., Xu, W., Wang, F., Gao, J., Li, Y., Li, M., Feng, Y., and Shi, G.: Machine learning combined with the PMF
- model reveal the synergistic effects of sources and meteorological factors on PM_{2.5} pollution, Environ. Res., 212, 113322,
- https://doi.org/10.1016/j.envres.2022.113322, 2022b.
- 2 Zhao, S., Yin, D., Yu, Y., Kang, S., Qin, D., and Dong, L.: PM_{2.5} and O₃ pollution during 2015–2019 over 367 Chinese cities:
- spatiotemporal variations, meteorological and topographical impacts, Environ. Pollut., 264, 114694,
- https://doi.org/10.1016/j.envpol.2020.114694, 2020.
- 665 Zuo, C., Chen, J., Zhang, Y., Jiang, Y., Liu, M., Liu, H., Zhao, W., and Yan, X.: Evaluation of four meteorological reanalysis
- datasets for satellite-based PM_{2.5} retrieval over China, Atmos. Environ., 305, 119795,
- https://doi.org/10.1016/j.atmosenv.2023.119795, 2023.